Electrical resistivity imaging of conductive plume dilution in fractured rock

Robin E. Nimmer · James L. Osiensky · Andrew M. Binley · Kenneth F. Sprenke · Barbara C. Williams

Abstract Electrical resistance tomography (ERT) was used to monitor a conductive plume dilution experiment that was conducted in fractured basalt in order to assess its applications in this type of fractured-rock environment. Tap water was injected into an injection well for 34 days to dilute a pre-existing potassium chloride (KCl) plume at a site in Idaho, USA. No further fluids were introduced artificially during a 62-day monitoring period. Both surface ERT and cross-borehole ERT were used to monitor dilution and displacement of the plume. A square grid of land-surface electrodes was used with the surface ERT. Three-dimensional images of surface ERT delineated areas of increased and decreased resistivities. Increasing resistivities are attributed to dilution/displacement of the KCl solution by tap-water invasion or the influx of seasonal recharge. Decreasing resistivities resulted from redistribution of residual KCl solution. Cross-borehole ERT was conducted between the injection well and each of seven surrounding monitoring wells. Polar plots of the injection-well resistivity data in the direction of each monitoring well delineate specific locations where tap water seeped from the injection well via preferential flow paths determined by time-dependent resistivity increases. Monitoring-well data indicate locations of clustered and isolated regions of resistivity changes.

Résumé La tomographie de résistivité électrique (ERT en anglais) a été utilisée pour surveiller une expérience de dilution d'un panache conducteur dans du basalte fracturé, afin d'évaluer son application dans ce type d'environnement à roches fracturées. De l'eau du réseau d'alimentation a été injectée dans un puits d'injection pendant 34 jours pour diluer un panache de chlorure de potassium (KCl) préexistant sur un site localisé dans l'Idaho aux Etats-Unis. Aucun autre fluide n'a été artificiellement introduit pendant une période de surveillance de 62 jours. L'ERT de surface et l'ERT entre puits ont toutes deux été utilisées pour contrôler la dilution et le déplacement du panache. Un maillage carré d'électrodes de surface a été utilisé pour l'ERT de surface. Des images tridimensionnelles obtenues par l'ERT de surface ont délimité des zones d'augmentation et de diminution de la résistivité. Les résistivités croissantes sont expliquées par la dilution/déplacement du KCl causés par l'invasion de l'eau du réseau ou par l'arrivée de la recharge saisonnière. Les résistivités décroissantes provenaient de la redistribution de la solution de KCl résiduelle. L'ERT de puits a été effectuée entre le puits d'injection et chacun des sept puits d'observation environnants. Des graphiques polaires des données de résistivité du puits d'injection avec la direction de chaque puits de surveillance, délimitent des zones spécifiques d'infiltration de l'eau du réseau à partir du puits d'injection via des trajectoires d'écoulement préférentiel déterminées par les augmentations de la résistivité dans le temps. Les données des puits de surveillance indiquent l'emplacement des zones amassées et isolées de variation de résistivité.

Resumen La tomografía de resistencia eléctrica (TRE) fue usada para supervisar un experimento de dilución de una pluma conductiva, que se realizó en un basalto fracturado, para evaluar sus aplicaciones en este tipo de ambiente de roca fracturada. Se inyectó agua del grifo dentro de un pozo de inyección durante 34 días, para diluir una pluma pre-existente de cloruro de potasio (KCl), en un sitio en Idaho, E.U.A. Ningún fluido adicional se introdujo artificialmente durante un período de monitoreo de 62 días. Tanto la TRE superficial, como la TRE de

Received: 10 January 2006 / Accepted: 8 January 2007
Published online: 30 January 2007

R. E. Nimmer (✉)
Hydrology Program, Department of Geological Sciences,
University of Idaho,
P.O. Box 443022, Moscow, ID 83844-3022, USA
e-mail: nimmer@uidaho.edu
Tel.: +1-208-8857714
Fax: +1-208-8857908

J. L. Osiensky · K. F. Sprenke
Department of Geological Sciences,
University of Idaho,
P.O. Box 443022, Moscow, ID 83844-3022, USA

A. M. Binley
Department of Environmental Science, I.E.N.S.,
Lancaster University,
Lancaster, LA1 4YQ, UK

Present address:
R. E. Nimmer · B. C. Williams
Department of Biological and Agricultural Engineering,
University of Idaho,
P.O. Box 440904, Moscow, ID 83844-0904, USA

 DOI 10.1007/s10040-007-0159-z

registro cruzado de pozo, fueron usadas para supervisar la dilución y desplazamiento de la pluma. Una malla cuadrada de electrodos de superficie se usó con la TRE superficial. Las imágenes tridimensionales de la TRE superficial delinearon las áreas de aumento y disminución de la resistividad. Se atribuyen las resistividades crecientes a la dilución/desplazamiento de la solución de KCl, por invasión del agua de grifo o por la entrada de recarga estacional. Las resistividades decrecientes fueron el resultado de la redistribución de solución de KCl residual. La TRE de registro cruzado de pozo fue ejecutada entre el pozo de inyección y cada uno de siete pozos de monitoreo circundantes. Las gráficas polare, de los datos del resistividad del pozo de inyección, en la dirección de cada uno de los pozos de monitoreo, delinean situaciones específicas dónde el agua de grifo se infiltra desde el pozo de inyección, siguiendo caminos de flujo preferenciales, determinados por los aumentos de la resistividad dependientes del tiempo. Los datos de los pozos de monitoreo indican sectores de cambios del resistividad en forma de racimo y regiones aisladas.

Keywords Fractured rocks · Basalt · Tracer tests · Electrical resistance tomography · Plume

Introduction

Fractured-rock environments contain contaminants in saturated and unsaturated zones in many areas of the world. Delineation of fracture zones is a crucial aspect of site and/or plume characterization, and, ultimately, is important to successful remediation efforts. Electrical geophysical methods have long been used in the mining and petroleum industries. As a relatively new method, electrical resistance tomography (ERT) has evolved into an important tool for site characterization at sites of groundwater and unsaturated-zone contamination. Specifically, surface ERT, which provides a three-dimensional image, is important to environmental investigations because all geological structures are three-dimensional as are current flow and potential distributions. Thus, a three-dimensional survey should provide more accurate, and more complete, images than two-dimensional surveys because out-of-plane current flow cannot be detected in a two-dimensional survey and, therefore, induces uncertainty and errors. Three-dimensional characterization is particularly important for fractured-rock characterization. The ERT methods provide cost-effective, supporting information for hydrogeological characterizations.

A field experiment consisting of two sequenced tracer injection tests was conducted in the unsaturated zone in fractured Columbia River Basalt. Figure 1 shows the site location and test plot layout of the experiment in Moscow, Idaho, USA. The test was divided into three phases. Phase 1 was designed to saturate fractures in the unsaturated zone with potassium chloride (KCl) solution. Based on previous hydrogeologic studies near the site (Li 1990), the solution was expected to flow approximately radially

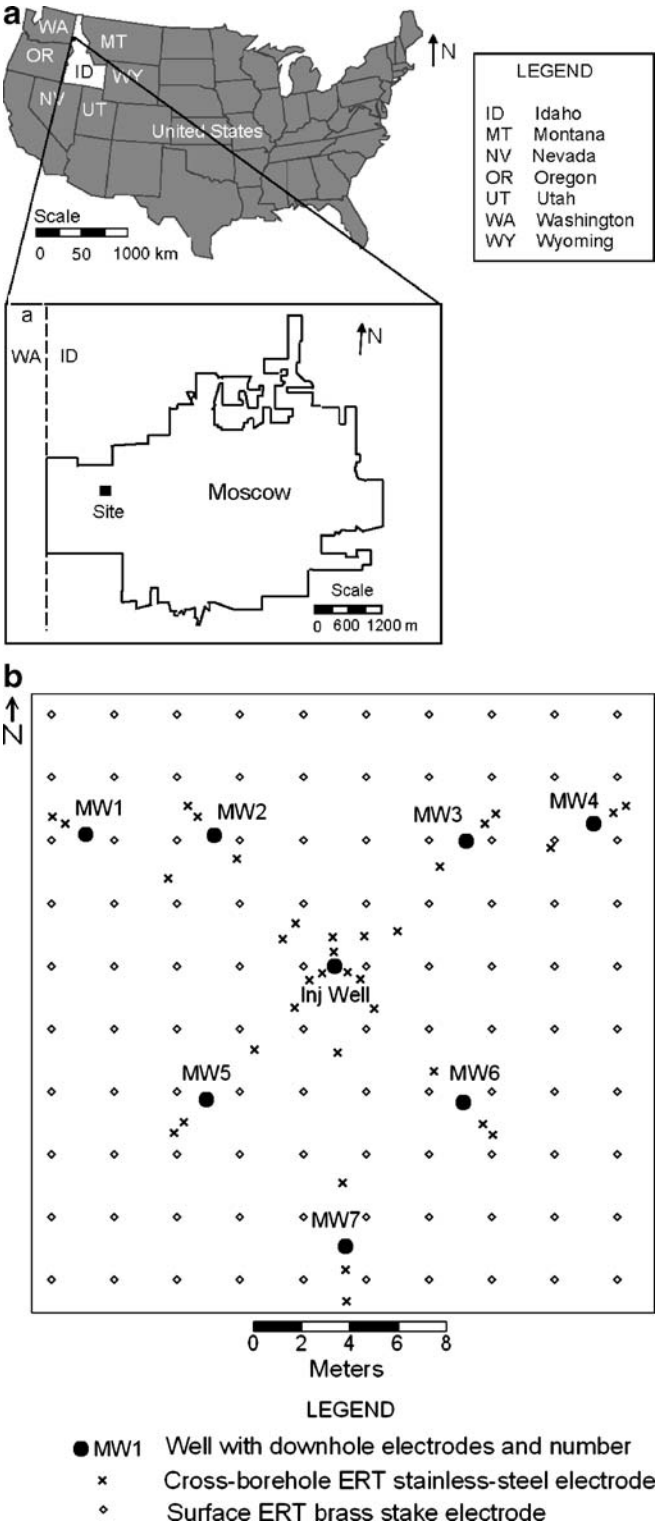

Fig. 1 **a** Map showing Idaho, USA and the study site at Moscow. **b** Location of wells and surface electrodes at the study site

away from the injection well through a number of mostly horizontal fractures of varying dimensions and degrees of connectivity. Over time, a conductive plume evolved in a hydraulically and electrically continuous pattern around the injection well. The Phase 1 state is referred to as "baseline" for the portion of the experiment described

 DOI 10.1007/s10040-007-0159-z

herein (76 days). Phase 2 was designed to test the suitability of various electrical methods to delineate spatial resistivity changes during in-situ dilution of the KCl plume by injection of tap water (34 days). Phase 3 was designed to measure resistivity variations in the fracture network during the post-injection monitoring period as the natural system rebounded (62 days).

Nimmer and Osiensky (2002a) presented results using hole-surface mise-à-la-masse (MALM) techniques for the first 34 days of phase 1 of the experiment. Nimmer and Osiensky (2002b) described the use of self potentials (SP), hole-surface MALM, and cross-hole MALM during the entire experiment. They found that the MALM method proved to be capable of tracking the evolution of the plume through to the end of the experiment, although dilution by tap water showed little change. Self potentials (SP) were affected by noise more than MALM, and SP alone did not provide enough information to delineate the tracer plume.

The ERT investigation described in this paper was designed to monitor changes in resistivity due to dilution and displacement of the KCl solution through the fractures during phases 2 and 3 of the tracer experiment. Surface ERT was used to image resistivity changes three-dimensionally and to explore the quality of information that this method can bring to fractured-rock characterization. Cross-borehole ERT between the injection well containing the source material (i.e., tap water), and seven nearby monitoring wells was used to provide information near the wells on the evolutionary plume dynamics at a more localized scale.

Electrical techniques

Surface electrical resistance tomography

Surface ERT is a three-dimensional, electrical, imaging technique where the electrodes are located at land surface arranged in a rectangular grid. In the technique, a two- to four-electrode array is used to measure a large number of resistances by applying sequences of exciting and recording potential differences to multiple electrode pairs within the electrode grid. These resistances are then inverted to generate a three-dimensional resistivity distribution. Three-dimensional surface surveys are becoming more common due to the ready availability of multi-channel resistivity transmitter/receivers to collect the data and faster computers to invert the data. Certainly, major advantages of this technique are the ease of set-up, high quality data, and non-invasive nature.

Surface ERT is also used for environmental applications. Industrial waste deposits and buried quarry geometry were imaged by Ogilvy et al. (1999) using surface ERT. Chambers et al. (1999) used the method successfully to image buried oil- and tar-contaminated waste deposits. Li and Oldenburg (1992) present results from an E-SCAN DC (direct current) resistivity field experiment based on a pole-pole measurement scheme and an inversion algorithm for three-dimensional problems. Park and Van (1991) described their inversion model and results from a large-scale, surface ERT experiment in unconsolidated materials involving the water infiltration. Park (1998) attempted to improve the inversion model and results of Park and Van (1991). Dahlin et al. (2002) showed that a three-dimensional roll-along technique in addition to surface ERT with three-dimensional inversion was successful in delineating the original locations of four abandoned, low-resistivity sludge ponds. No studies in the literature were found using surface ERT to analyze tracer experiments.

Cross-borehole electrical resistance tomography

Cross-borehole ERT provides images of the subsurface resistivity distribution in the intervening space between at least two wells. A four-electrode array is used to measure a large number of resistances by applying sequences of exciting and recording potential differences to multiple electrode pairs, where most of the electrodes are located downhole. The resistance data are inverted to generate a cross-sectional resistivity distribution or tomogram. Electrodes are placed downhole and, possibly, also at land surface. Resolution of ERT is a function of electrode geometry, data accuracy, and measurement schemes, among other factors (Daily and Ramirez 1995). Advantages of ERT over other electrical resistivity methods in the context of this paper are its enhanced vertical resolution and accuracy.

Cross-borehole ERT has been used for over a decade in environmental investigations. Typical cross-borehole studies include leak detection (Daily et al. 1995a; Ramirez et al. 1996), fluid or contaminant migration (Daily et al. 1992, 1995b), remediation (by steam or air injection) monitoring (Ramirez et al. 1993; Daily and Ramirez 1995; LaBrecque et al. 1996; Lundegard and LaBrecque 1995), and evaluation of engineered hydraulic barriers (Daily and Ramirez 2000; Slater and Binley 2003). More recently, research has been conducted in applying cross-borehole ERT results to determine tracer concentrations using a linear relation (Kemna et al. 2002; Singa and Gorelick 2005).

A small number of cross-borehole ERT studies have been conducted in fractured rock. This method was used by Slater et al. (1997a) to image salinity change, and identify fracture zones in limestone. Slater et al. (1997b) examined unsaturated zone transport mechanisms through the use of cross-borehole ERT during an infiltration tracer test conducted in the unsaturated zone in chalk. Zaidman et al. (1999) used cross-borehole ERT in unsaturated chalk during a surface infiltration experiment to simulate the effects of heavy rainfall.

Local geology and hydrology

The experiment was conducted at an unsaturated-zone field site on the University of Idaho campus in Moscow, Idaho, along the eastern edge of the Columbia River

 DOI 10.1007/s10040-007-0159-z

Plateau. The experiment was completed in the uppermost basalt flow (i.e., the Lolo Flow of the Priest Rapids Member) of the Wanapum Formation. The Lolo Flow has a depth in the study area of approximately 3 to 61 m and dates to 14.5 million years ago (Bush and Seward 1992). Bush and Seward (1992) describe a typical Columbia River Basalt flow as consisting of (from top to bottom) a vesicular flow top, entablature, colonnade, and pillows. However, Li (1990) describes the structure of the Lolo flow as having lateral variations. In addition, the typical, six-sided columns are not well formed.

The Lolo basalt flow is covered by about 2 m of alluvial sediments and Pleistocene Palouse loess (Provant 1995) at the test site. The alluvial sediments consist of reworked loess with basalt and granite fragments. The loess is composed of a silty loam with predominantly quartz and feldspar in addition to small percentages of sand and clay. An approximately 0.5-m-thick layer of silty clay forms the sediment-basalt contact at the research site.

The wells drilled for this investigation were completed near the basalt flow top, which is weathered, fractured, and vesicular. Weathered basalt results from alteration by water flow through fractures and forms halloysite clay. Although fractures increase the hydraulic conductivity of the rock, clay may infill the fractures reducing rock permeability and may provide a limited site for ion exchange. Clay also fills some of the vesicles. Consequently, flow tops generally impede vertical flow; however, the fractures become cleaner (i.e., less weathered) with depth. A certain number of horizontal fracture zones may be laterally continuous for several meters; however, smaller fractures predominate. Vertical joints may connect the horizontal fractures. The monitoring wells were likely connected to both clean and clay-filled fractures, in addition to dead-end and interconnected fractures. There have been no other data collected in this area at the depths of interest to this study.

Experimental method

Field-site logistics

Eight wells, each with a diameter of 15.2 cm (6 inches), were drilled by air-rotary (no water was added) to varying depths, with the distribution shown in Fig. 1b. Prior to the KCl injection, the water table initially was located at the bottom of the deepest well, MW1 (774.75 m above mean sea level (MAMSL) or 7.49 m below land surface). Figure 2 shows the well logs for the eight wells and illustrates the lithologic heterogeneity at the site, which can be used to infer heterogeneity that governs fate and transport. The term "basalt" in this figure represents basalt that is either massive (unfractured), or vesicular and/or fractured, but where the fracture surfaces have not been substantially altered by weathering processes. The monitoring wells penetrated various fractures containing perched groundwater such that a few centimeters of standing water collected in the bottoms of all of the wells after drilling. The wells were cased with 15.2-cm diameter PVC pipe through the sediments and left as open hole within the basalt. An inner PVC liner with a diameter of 5.1 cm was placed in each monitoring well; the bottom end of the pipe was left uncapped, and hacksaw slots were made in the bottom 10 cm to allow water to enter the pipe for water sampling. Copper, downhole electrodes were attached to the outside of each PVC liner. Each monitoring well annulus was filled with a 10-cm-long sand pack followed by dampened silt to the land surface to establish an electrical connection between the electrodes and the basalt medium. Electrodes in the injection well were attached to 1.3-cm diameter PVC plastic pipe and centered in the borehole. The soil around each well was mounded and covered with plastic sheeting to divert precipitation and surface runoff away from the backfilled annulus.

Surface and cross-borehole ERT were used to monitor changes in electrical resistivity within the well field over time. For cross-borehole ERT, the injection well was

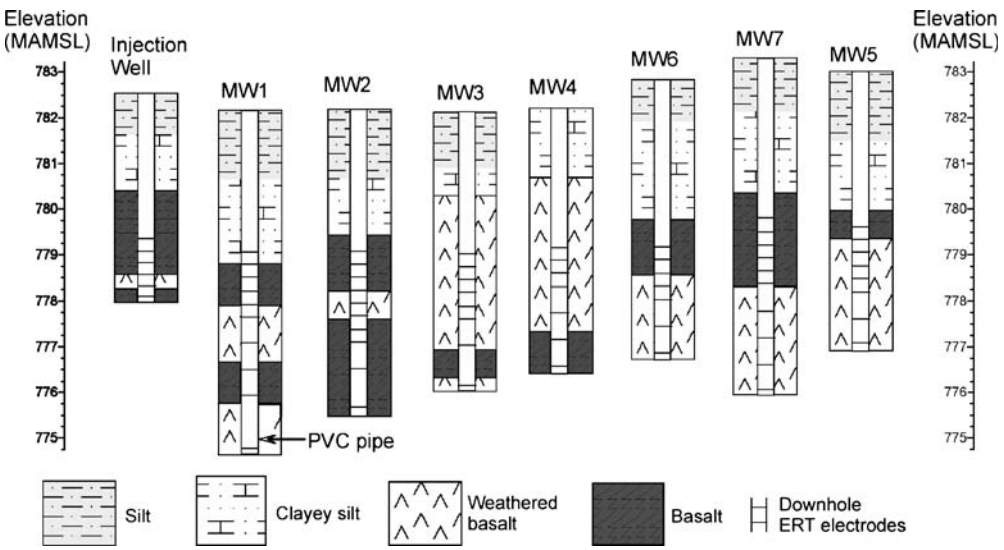

Fig. 2 Well logs for monitoring wells and the injection well (modified from Nimmer and Osiensky 2002a). Electrode locations are also shown

 DOI 10.1007/s10040-007-0159-z

paired with each of seven monitoring wells, generating seven data sets per day of data collection. A pole-pole configuration was used for both methods. The reference electrode consisted of a porous pot, and the distant current electrode consisted of three stainless-steel stakes connected by a copper wire. These electrodes were placed 74.5 m to the west and 62.4 m to the southwest of the injection well, respectively, due to land-use constraints. The reason for the close proximity of the distant electrodes to one another was the intended placement of a north-south trending fence near the east side of the trailer to cordon off the field site from cows. The cows were relocated so the fence was not installed.

A uniform grid of 10×10 brass surface-stake electrodes was placed in the center of the well field for the surface ERT segment of the experiment. The electrodes were located 1.3 m apart and arranged as shown in Fig. 1b. These electrodes were wired directly to a multi-electrode cable system attached to a transmitter/receiver system.

Sixty-six downhole copper electrodes and 34 surface stainless-steel stake electrodes were used in the cross-borehole ERT portion of the experiment (Figs. 1b and 2). The downhole electrodes consisted of 14-gauge copper underground feeder cable wrapped around the each PVC liner to approximate point electrodes. The downhole electrodes were placed 10 cm from the bottom of each well and at 30 cm intervals to the top of basalt. Only 66 of the total 89 downhole electrodes were used due to the limited number of available circuit switches. The study originally was designed for hole-hole and hole-surface MALM experiments. After electrode placement, cross-borehole ERT was added to the study scope to help provide better vertical definition of potential flow paths. The surface stake electrodes were located along the plane between the injection well and each monitoring well, and were placed such that two electrodes were located on the outside (i.e., beyond) of each well and two were located between the wells for a total of six electrodes per array. These electrodes were spaced on multiples of 30 cm. The land-surface and downhole cross-borehole ERT electrodes were also wired directly to a multi-electrode cable system attached to a transmitter/receiver system.

Pre-experiment conditions

Phase 1 of the experiment was represented by development of the initial conditions for phase 2. Baseline electrical conductivity of the water in the bottom of the injection well prior to phase 1 was 0.1153 S/m. Phase 1 (t=−76 d) (negative value indicates days before the beginning of the experiment) began when the injection well was filled with 34.8 L of KCl solution with a constant electrical conductivity of 0.60 S/m from a heated polyethylene storage tank. The actual concentration was not measured, but the total dissolved solids (TDS) were between 3.30 to 4.50 mg/L. This KCl solution is a relatively dilute solution compared to other experiments (e.g., Slater et al. (1997b) conducted an experiment with a NaCl conductivity of 8 S/m), and should not have substantial density effects. The solution was heated to maintain a temperature of approximately 10°C. A total of 765 L of solution was added to the injection well over the 76 days at an average rate of 10.07 L/d. A 1.91-m-long column of conductive fluid was maintained from the bottom of the well to the top of the basalt layer 2.67 m below land surface. A constant water level in the injection well was maintained at an elevation of 780 m above mean sea level (AMSL) through a drip system.

Experiment conditions

Phase 2 began at t=0 d when the KCl solution was pumped out of the injection well, and the well was refilled to the same elevation with tap water (electrical conductivity of 0.0294 S/m). A total of 221 L of tap water was injected over 34 days, thereby displacing and diluting some of the KCl solution in the fracture network. At t=34 d, the tap-water injection ceased. Data collection continued for the next 62 days as phase 3 of the investigation until t=96 d.

Site characterization and conceptual model

During phase 1 of the experiment, an air-filled borehole in the unsaturated zone was filled with a KCl solution, and saturation of the fracture network began. Fluid was anticipated to flow out of the well approximately radially through larger fracture zones connected by a network of smaller features based on a hydrogeologic study by Li (1990) conducted at a site approximately 100 m to the east and on nearby outcrops. It is likely that some of the fluid also drained from the bottom of the borehole. Clay resulting from weathering of the basalt may have reduced the hydraulic conductivity of some of the fractures. Over time, a continuous fracture network was assumed to have been saturated with KCl solution with diffusion occurring between the fractures and the basalt matrix based on the duration of the injection. Results from the borehole-surface and borehole-borehole MALM data (Nimmer and Osiensky 2002a, 2002b) indicated that the conductive fluid did migrate in a nearly radial pattern away from the injection well but flowed mostly to the north in an area roughly encompassing MW1 to MW3 and also toward MW6 and MW7. The northerly flow direction mimics the topography. Unfortunately, due to current loss in bundled wires, the ERT data during phase 1 of the experiment is unusable.

During phase 2 of the experiment, the injected tap water was expected to follow the same pathways as the KCl, although the physics of the migration was anticipated to be different. Specifically, reversing the concentration gradient would by matrix diffusion and diffusion from solution in the vesicles and dead-end fractures cause the conductivity of the tap water to increase. The MALM data again demonstrated the northerly flow direction during phases 2 and 3 but with depressed voltages (i.e., decreasing resistances). These depressed voltages may have been related to a decrease in current density over

 DOI 10.1007/s10040-007-0159-z

time with the growth of the plume. The MALM method was concluded to be insensitive to plume dilution by tap water resulting from far fewer data points than with other methods. This result is inherent with the use of surface electrodes and weak conductivity contrast of the waters.

Data collection and processing

Surface ERT resistance (R) measurements were collected infrequently due to lengthy setup and take-down time, as well as weather problems. One data set was collected during each of the experimental phases (i.e., three times). Because collection of complete, surface ERT data sets is very time consuming, an alternative measurement scheme was applied. This scheme is called the "cross-diagonal survey" method (Loke and Barker 1996). In this method, the potential measurements are collected along the x- and y-directions and along 45° diagonal lines from the current electrode rather than from all possible grid locations. This result reduces the total number of measurements by approximately one third (Loke and Barker 1996). Current was injected at each of the brass surface electrodes, and resistances were measured at the electrodes in the x- and y-directions, and along 45° diagonal lines crossing through each current electrode. This procedure kept the data-collection time manageable. Each of the data sets consisted of 2,940 measurements (including reciprocals), requiring a total of approximately 13 h including setup and disassembly. The electrodes were installed and removed for each measurement cycle to preclude interference with other electrical methods of data collection (e.g., MALM and SP). Markers were placed at the locations of the electrodes to ease setup for each subsequent measurement period.

Cross-borehole ERT data were collected eight times during phases 2 and 3 of the experiment; however, only four data sets are presented here to simplify visualization; the other four data sets do not provide additional, significant information. The first set of ERT measurements taken at t=4 d for all seven injection well-monitoring well pairs—Injection(I)-M1 through I-M7—in sequence are considered to represent baseline conditions to allow evaluation of changes over time. Each complete data set of 2,830 measurements (including reciprocals) was collected in approximately 9 h through a supervised, programmed switching system.

Data errors

Resistances were calculated from voltages for a four-electrode array. Reciprocals were examined to quantify the transfer resistance errors. A transfer resistance is the resistance between the potential electrode and the reference electrode. In this experiment, only positive current electrodes and potential electrodes were switched. Reciprocals should provide the same transfer resistance value (Binley et al. 1995). Reciprocal errors were quantified (as a percentage) based on

$$\%\ \text{Error} = \frac{\left|R - R_{recip}\right|}{R_{mean}} 100, \tag{1}$$

where R is the resistance, R_{recip} is the reciprocal resistance, and R_{mean} is the mean of the two resistances. Data with reciprocal errors greater than 5% were culled, and common data sets between the same well pairs were developed for comparison purposes. Table 1 lists measurement information for the inversion process for the cross-borehole data between the injection well and each monitoring well, and for the surface survey.

Resistivity determination

After the data errors were filtered out, resistance ratios (R_{rat}) were calculated. Resistance ratios were generated by

$$R_{rat} = \frac{R_{t2}}{R_{t1}} R_h, \tag{2}$$

where R_{t1} is the transfer resistance at time t_1, R_{t2} is the subsequent transfer resistance at time t_2, and R_{h} is the transfer resistance for the comparable homogeneous resistivity distribution (100 Ωm; ohm-meters) predicted by the forward model. This equation is based on the method described by Daily et al. (1995b). The RES3DMOD code (Loke 2001) was used to generate the R_{h} values for the surface ERT data. A proprietary finite-element based DC resistivity forward model (A. Binley, Lancaster University, Department of Environmental Sciences, unpublished data, 2000) was used to generate the R_{h} values for the cross-borehole ERT data. The R_{rat} values were input into the inversion models that generated resistivity values (ρ).

Resistivity inversion

Two-dimensional, finite-element grids were developed for the forward models and inverse models for analysis of the cross-borehole ERT data. The grid for each I-MW (injection well–monitoring well) pair is unique due to site-specific minor land-slope variations, variable well depths, and different numbers of electrodes and electrode locations. Each grid consists of a subgrid, which extends

Table 1 Resistance measurements for inversions

	Cross-borehole survey - monitoring wells							Surface survey
	MW1	MW2	MW3	MW4	MW5	MW6	MW7	
Total number of measurements (includes reciprocals)	462	462	380	342	380	342	462	2,940
Percentage of measurements used	73	79	70	87	78	93	85	75

 DOI 10.1007/s10040-007-0159-z

from land surface to the bottom-most electrode. Figure 3 shows the subgid for well pair I-MW1. For this example, the elemental spacing in the x-direction is 0.3 m and the z-spacing (vertical) within the electrode portion of the subgrid is 0.15 m. Due to the gently sloping topography, the land-surface elevation was calculated by averaging the elevations of each I-MW well pair. The spacing in the z-direction above the electrode portion of the subgrid to land surface is this separation distance divided by 10; each grid then contains 10 rows of elements above the uppermost electrode of both wells. These spacings range from 0.2748 m for I-MW3 to 0.3096 m for I-MW6. Beyond the subgrid, cell sizes increase incrementally to a maximum cell size of 100 m to provide a grid space for placement of the remote electrodes and application of the boundary conditions.

The electrode spacing was not ideal for cross-hole ERT due to the original design of the experiment (that is, specifically for MALM and surface ERT), resulting in poor resistivity sensitivity between the wells; however, the inversion results give good vertical definition of resistivity changes at the wells. Consequently, only data near the electrode column are analyzed.

Two different inversion codes were used to invert the cross-borehole and surface ERT data. The surface data were inverted using the RES3DINV (Loke 2001) code and included topographic corrections, as well as the exact locations of the distant electrodes. A proprietary code (same as used for the forward model) was used to invert the cross-borehole data. The proprietary inversion model is designed to reproduce the measured potential field by using a theoretical relation based on Occam's approach of deGroot Hedlin and Constable (1990); RES3DINV uses this same method with modifications described by Sasaki (1992). The area under investigation is parameterized based on the finite-element grids. The resistivity distribution is solved by the model using a minimization of the objective function

$$\Phi(m) = [\mathbf{D} - \mathbf{F}(m)]^T \mathbf{W}^{-1} [\mathbf{D} - \mathbf{F}(m)] + \alpha m^T R m \qquad (3)$$

where $m = log_e(\rho^{-1})$, $\mathbf{D}$ is the vector of measured resistance, $\mathbf{F}(m)$ contains the corresponding forward model resistances due to parameter m, T is the matrix transfer, $\mathbf{W}$ is a vector of data variances used to weight individual measurements, R is a roughness matrix used to force smoothing of the resistivity distribution and to stabilize the inverse solution, and α is a smoothing parameter. An iterative solution is reached when the data misfit is minimized to an acceptable level.

Injection well resistivity values are plotted at specific depth intervals as polar charts in the radial direction of each monitoring well from the injection well to evaluate the locations of potential fluid pathways (i.e., fracture zones) during tap-water injection. The measurements represent a distance of 0.224 m into the formation, calculated by subtracting the well radius from the grid element size. The polar plots show directional resistivities, which could not have been derived from single-well experiments. Monitoring well resistivities are presented as graphs of resistivity (by grid-element elevation) versus time; resistivity values are taken from grid elements that border the inner subgrid side of the downhole electrodes (Fig. 3). Interpretations are based on the assumption that changes in resistivity values are due strictly to changes in pore-water resistivity or degree of saturation.

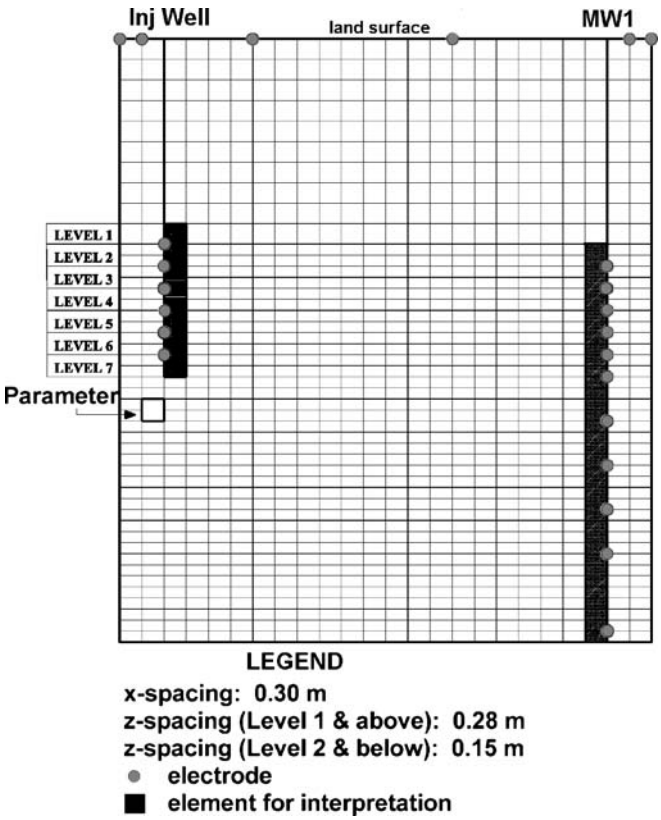

Fig. 3 Example cross-sectional subgrid for I-MW1

Hydrologic data analysis

Hydrologic data collected over the duration of the experiment at and near the field site provide information in support of the electrical data interpretation. Water levels were measured in each of the eight wells. Precipitation data in water equivalents for Moscow were provided by R.J. Qualls (Idaho State Climatologist, personal communication, 2005).

Figure 4a shows the elevation of water levels in the wells, and daily amounts of precipitation. Water levels in the monitoring wells were fairly stable from the beginning of phase 1 (t=−76 d) through at least t=4 d (the beginning of phase 2). Between t=4 and t=15 d (phase 2), water levels began to rise in all the monitoring wells. This rise is believed to be caused by the infiltration of water from snowmelt and heavy rain. Precipitation events correlate well with increases in water levels in the monitoring wells. Water levels peak at approximately 66 d, but are not

 DOI 10.1007/s10040-007-0159-z

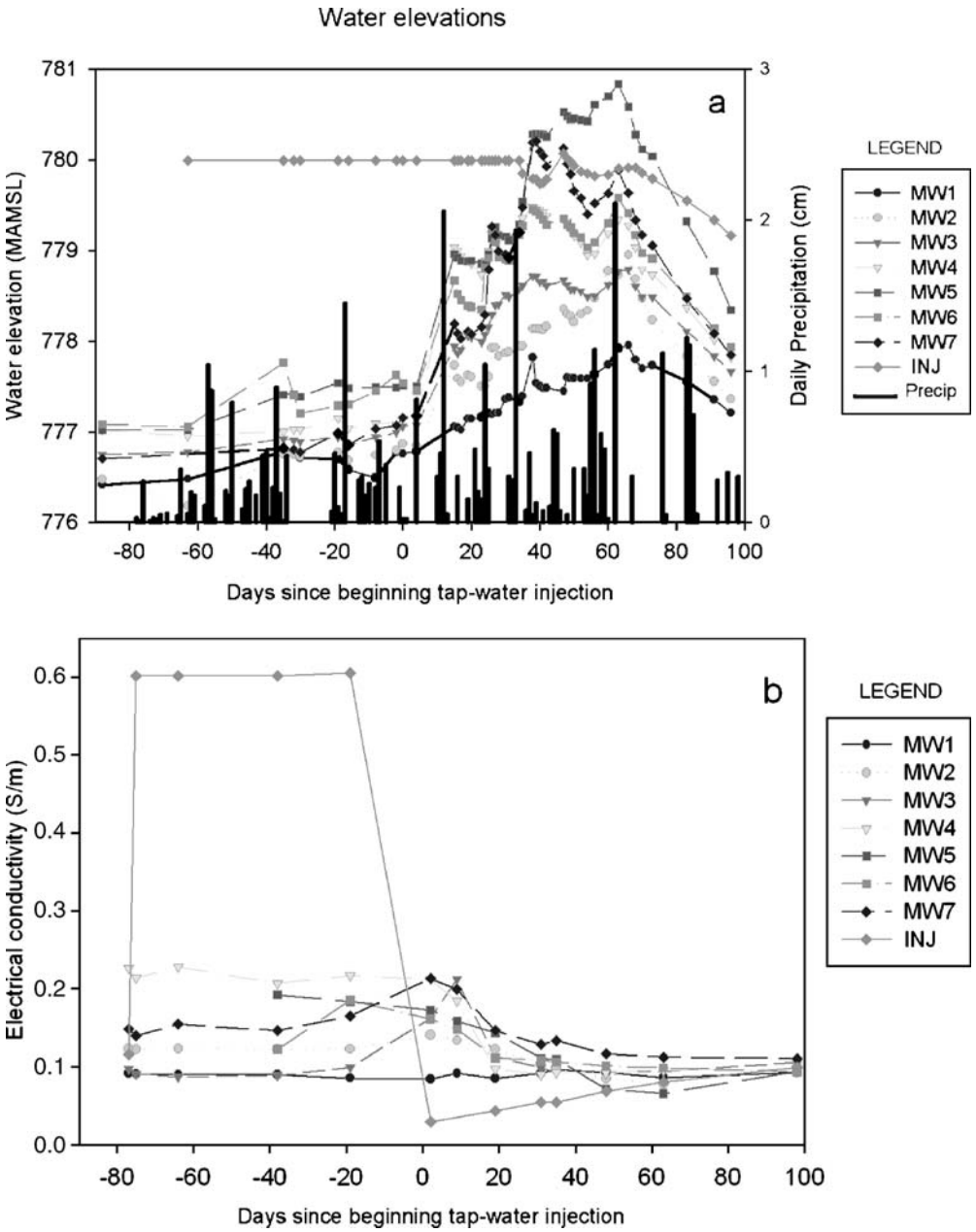

Fig. 4 **a** Graph of water-elevation measurements in the wells and precipitation in water equivalents. **b** Graph of electrical conductivity measurements of water in the wells. Day *0* represents the beginning of the tap-water injection

associated with a single, major precipitation event or a significant increase in the duration of precipitation. Coincidently, the tap-water injection phase of the experiment concluded shortly before water levels in MW5 and MW7 rose above the water-level elevation in the injection well. It is important to note that water levels in the injection well remained fairly constant until approximately t=78 d. Electrical conductivity (EC) of the well waters was measured throughout the experiment (Fig. 4b). EC of the groundwater in the monitoring wells began to increase following the injection of KCl solution, indicating arrival of the plume. Based on hypothetical modeling of variable conductivity borehole fill (personal observations), one order of magnitude change in the borehole fluid conductivity should have very little effect on the inversion results. The EC then decreased prior to tap-water injection (phase 2), or shortly thereafter, resulting from the recharge of lower conductivity water.

Groundwater-elevation contour maps interpolated from water-level data measured in wells at the field site are shown for four time-periods in Fig. 5. The hydraulic gradient flattens after t=30 d due to the rising water table but remains steep toward the northwest direction. After t= 52 d, water is flowing away from MW5, generally mimicking the sloping topography toward the north with a few meters offsite toward the west. By t=96 d, the water-level high returns in the injection well. This high may be due to the shallow depth of the injection well in comparison to the monitoring wells, given that it is unknown when the water level in the wells represented

 DOI 10.1007/s10040-007-0159-z

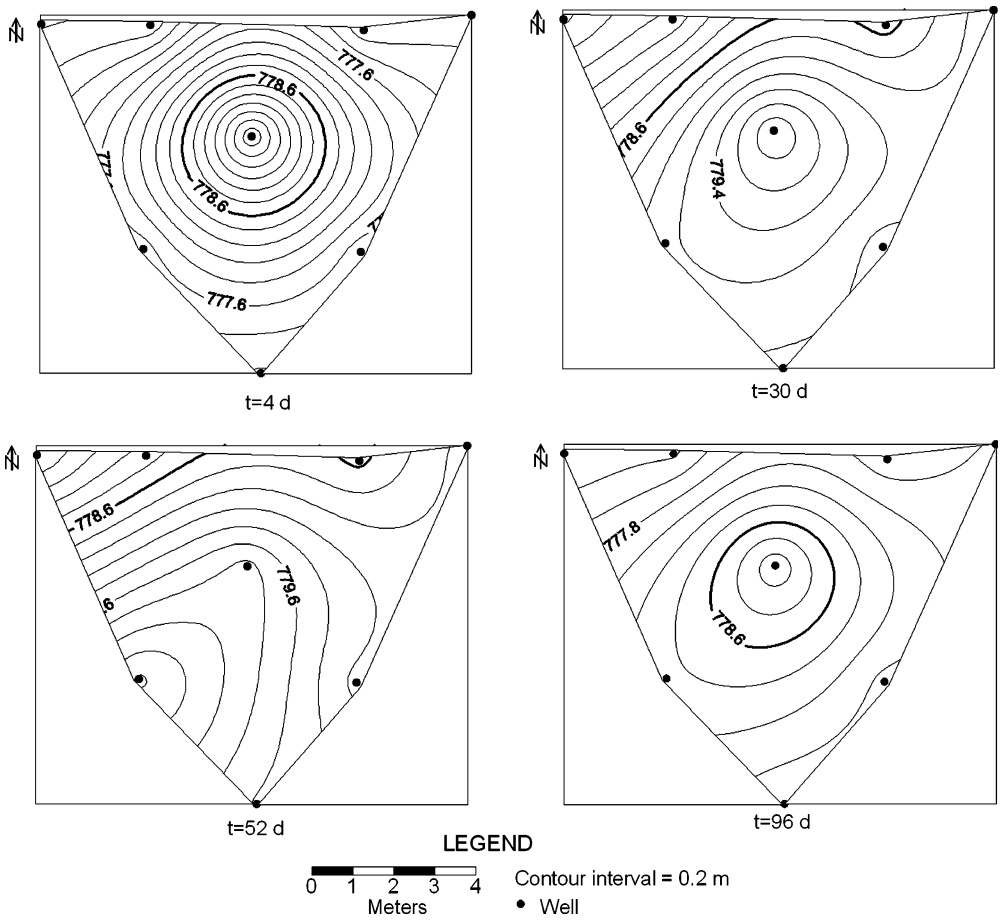

Fig. 5 Groundwater elevation contour maps at the experiment site. Elevations are in meters above mean sea level (MAMSL). *Thick line* represents the elevation contour line 778.5 m for reference purposes. See Fig. 1 for well locations

the true water table and at what time the water levels may not have represented the true water table.

Surface ERT results and discussion

Surface ERT data were collected on two occasions during this investigation. The first data set was collected at t= 17 d (phase 2). The second data set was collected at t= 68 d (phase 3). To evaluate the resistivity changes caused by water conductivity and saturation changes, percent changes in resistivity are examined. Figures 6 and 7 show the resistivity values for (t=68 d/t=17 d) as images in map view and cross-section view, respectively. Areas of a positive percent change indicate an increase in resistivity since t=17 d.

Figure 6 shows that the subsurface is heterogeneous over short distances based on the resistivity variations. Layer 1 has a low resistivity anomaly trending nearly north-south through the center of the electrode area with the lowest resistivities in the southern half of the anomaly due to an increase in saturation caused by the spring snowmelt and rains. Zero percent change is shown in the area of the injection well in layer 3 (bulk of the injection zone). As expected, resistivity changes occurred in areas outside the vicinity of the injection well; the high resistivity anomalies detected in layers 2 and 3 at the northern and southern areas of the site likely reflect the influx of lower conductivity recharge water displacing higher conductivity in-situ water at these locations. Low resistivity anomalies in the deeper layers in the southeast quadrant of the site probably reflect redistributed residual KCl solution.

Figure 7 shows the resistivity variations with depth. There appears to be no correlation between resistivity and lithology (Fig. 2). This result may be due to the gradational lithologic boundaries and the electrical data presentation as changes in resistivity and not raw resistivities. The cross-sectional images show a resistivity discontinuity at a depth of approximately 1 m. This discontinuity is attributed to the aforementioned clay layer present at the top of the basalt within the test site. However, the clay layer appears to be discontinuous in the southernmost parts of the test site. These areas may provide more direct pathways of infiltrating recharge water. The resistivity distributions in the deeper layers suggest that higher resistivity water exists in the northeastern part of the site.

Cross-borehole ERT results and discussion

Injection well

Figure 8 depicts resistivities for grid elements along the axis of the injection well. These resistivities are presented

 DOI 10.1007/s10040-007-0159-z

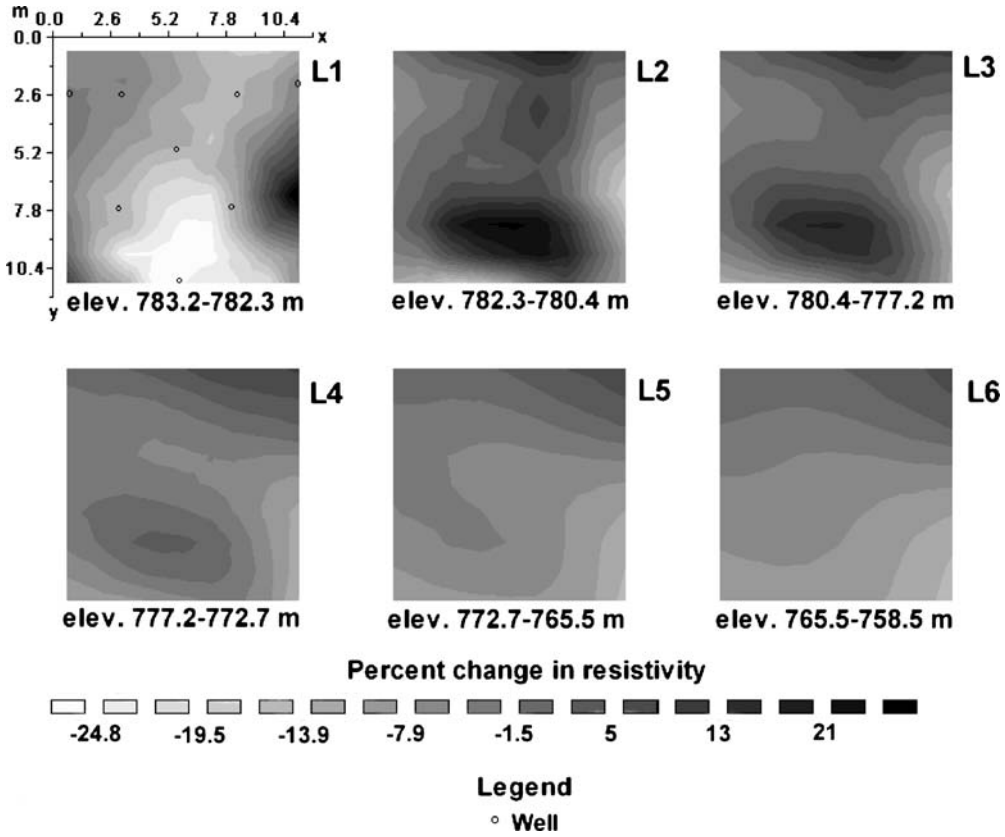

Fig. 6 Surface ERT resistivity distributions for t=68/t=17 d (land surface is at an elevation of 783.2 MAMSL): map-view images (*north is up*). The northwestern-most electrode is represented by (0,0). Layer thickness increases with depth. *L* stands for layer. See Fig. 1 for well descriptions

in polar-plot form for phase 2 of the cross-borehole ERT experiment; the values constitute changes from cross-borehole baseline (t=4 d) in directions toward the monitoring wells for t=15 d, t=26 d, and t=34 d. Each spoke in the polar plots represents a line connecting the injection well and a different monitoring well. Resistivity values are presented for seven levels in the injection well based on the model grid (Fig. 3). Each level represents a 30-cm-thick zone, except for level 1, which is approximately 15 cm thick as explained earlier. A positive percent change depicted in Fig. 8 indicates that this zone is more resistive than baseline. Figure 4b shows that the electrical conductivity of water in the injection well increased continuously during the injection phase, from 2.94×10^{-2} to 5.42×10^{-2} S/m, most likely by desorption/diffusion of the residual KCl solution from the vesicles, dead-end fractures, and the basalt matrix. The rate of tap-water movement out of the injection well was very slow (average rate of 6.5 L/d).

Figure 8 illustrates the heterogeneous nature of electrical resistivity changes in the fractured basalt. Locations adjacent to the injection well with significant increases in resistivity during the tap-water injection phase most likely indicate the presence of fluid transmitting fractures. Large, early-time, resistivity increases were detected in levels 3 and 4 in the direction of MW7, level 5 in the direction of MW1, and level 7 in the direction of MW6. These resistivity increases most likely represent areas invaded by higher resistivity water. Late-time resistivity increases such as those in levels 1, 2, 4 and 5 in the direction of MW3, all of the level 7 directions, and in level 1 in the direction of MW5, may indicate sparsely fractured areas with predominately matrix flow. Locations where the resistivity values did not continue to increase significantly after t=15 d may represent zones flushed of KCl solution at an early time (i.e., levels 3 and 4 in the direction of MW7). Decreased resistivity values detected at t=15 d in levels 1 and 2 in the direction of MW7 are likely due to diffusion of KCl solution back into the injection well from dead-end fractures and pores.

Monitoring wells

Inverted monitoring well resistivity values for phases 2 and 3 are shown in Fig. 9 as line graphs of element elevation versus percent change in resistivity for four data sets. Examination of details about the resistivities, elemental tendencies of the data by time, and how the data are clustered provide insight into the changes in resistivity caused by the dilution and redistribution of the KCl plume.

The percent change of resistivities since baseline illustrate whether the resistivities have increased or decreased. Values approximating 0% change at early times represent areas of little change (e.g., MW2 and MW3). Resistivities with a negative percent change may be due to redistribution of the in-situ KCl solution. Conversely, resistivities with a positive percent change indicate areas of shorter and/or faster flow paths, where dilution of the existing KCl solution is caused by mixing with tap water

 DOI 10.1007/s10040-007-0159-z

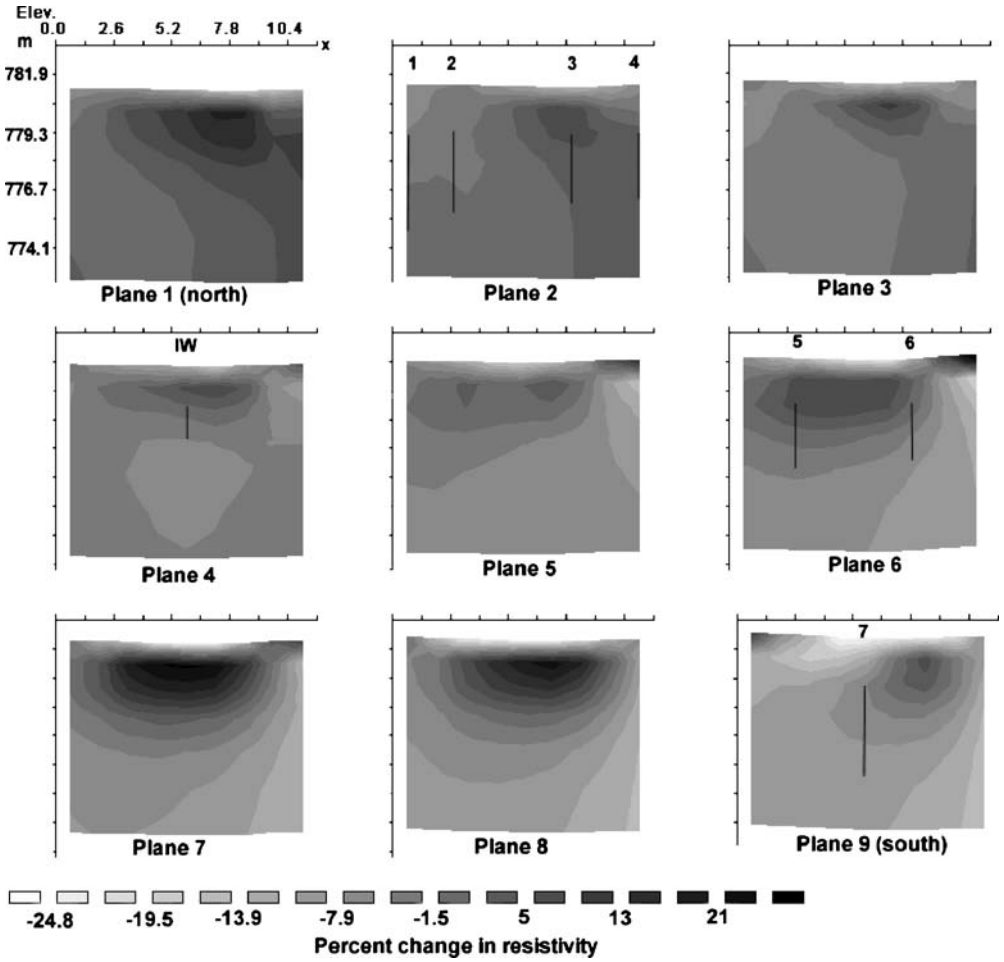

Fig. 7 Surface ERT resistivity distributions for t=68/t=17 d (land surface is at an elevation of 783.2 MAMSL): cross-sectional images. The thickness of each plane is 1.3 m. *Lines* on cross sections represent depths of electrode sections, and the *numbers* correspond to the well number (i.e., MW1 is represented by *1*). When wells are located along the border of two cross-sections, the electrode lines are located on the northernmost cross-section. See Fig. 1 for well descriptions

or recharge water. Areas where resistivities varied little with time (e.g., MW6 elevations 777.8 m and below) indicate points of stagnation within the fracture system.

Specific locations (i.e., elevations) of resistivity changes over time within each well are delineated in Fig. 9. Water from some of the monitoring wells became more resistive, whereas water from other wells became less resistive over time. Data that indicate similar increasing or decreasing tendencies may represent similar flow conditions (e.g., upper and lower portions of MW2). Zones showing increasing resistivities delineate dynamic pathways for resistive water movement. MW2, MW3, MW4, and MW5 contain significantly greater numbers of grid elements with increasing resistivity patterns compared to MW1, MW6, and MW7. These findings support the surface ERT data. At elevation 780.1 m in MW7, an increasing resistivity tendency began with a positive percent change; however, this elevation is 0.1 m above the constant head in the injection well, which strongly suggests that the increasing resistivity tendency was caused by factors other than tap-water injection. Wells with increasing resistivities in the upper elevations may indicate dilution by recharge from surface infiltration (i.e., upper halves of MW2, MW3, and MW5). The range of resistivity values at a single elevation does not span more than approximately 40 Ωm except for elevation 777.5 m in MW3 that increased nearly 80 Ωm. This result is indicative of fracture flow and tap-water dilution. Zones showing decreasing resistivities delineate areas of relatively slow moving water; these areas reflect spatial redistribution of residual KCl solution over time. Zones showing decreasing resistivities tend to have more sporadic responses and are generally deeper in succession. Water from MW7 contains the lowest resistivities. Zones with alternating increasing and decreasing resistivities (e.g., bottom half of MW3) may reflect hydraulic gradient fluctuations shown in Fig. 5. Zones with no definitive patterns correspond to the complex nature of the hydraulics and fracture system.

Relations were examined between the cross-borehole ERT resistivity changes and well logs (Fig. 2). Varying data were anticipated based on specific lithologic units; for example, isolated resistivity changes in “basalt” representing flow-through clean, individual fractures, or a lack of resistivity changes in “basalt” in unfractured zones. However, there does not appear to be a clear-cut correlation between the resistivity data and lithology. Given the lack of a relation and because resistivity

 DOI 10.1007/s10040-007-0159-z

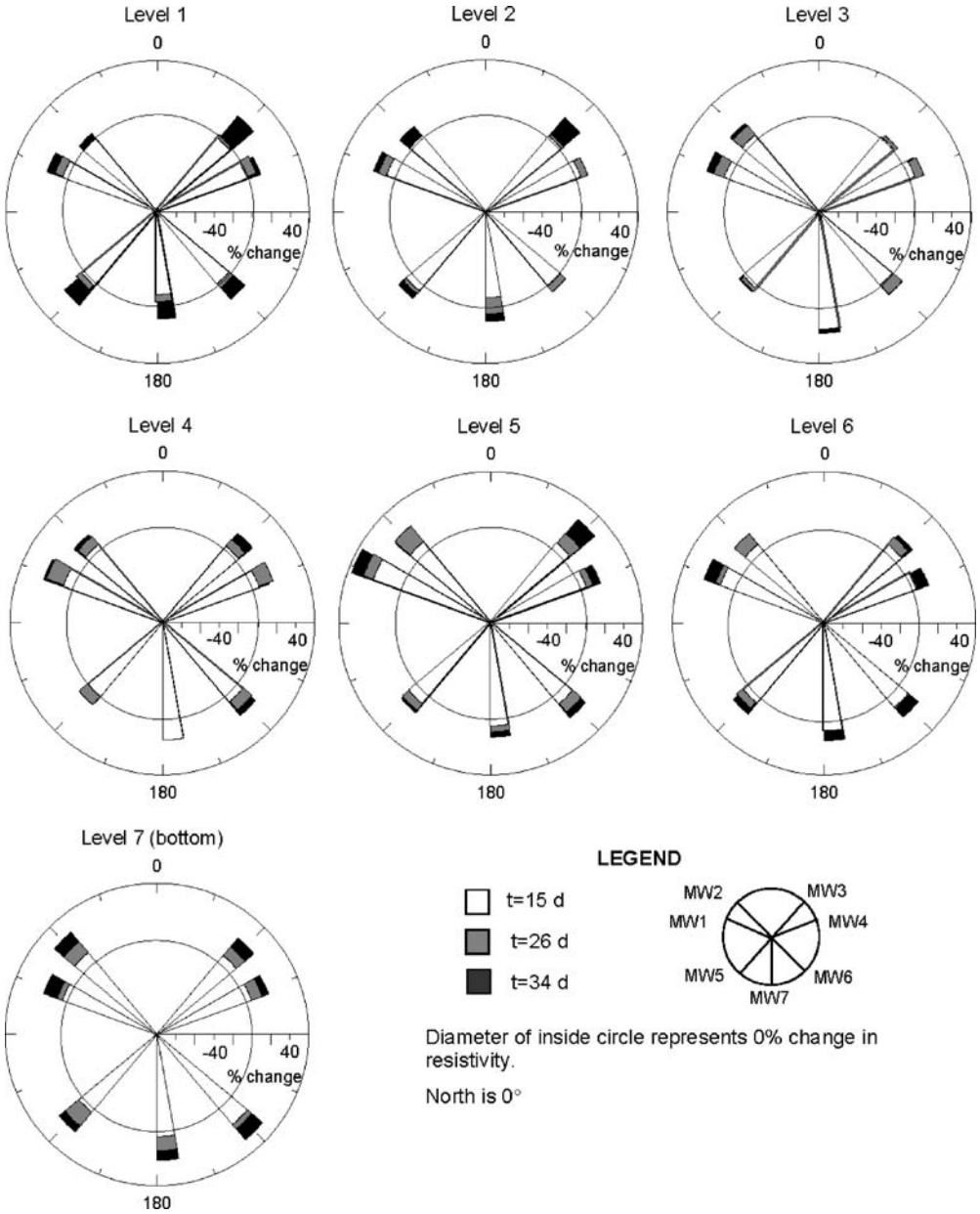

Fig. 8 Polar plots of injection well resistivities as percent change from baseline for elements adjacent to the borehole within the subgrid region for the cross-borehole ERT experiments. A negative change is a reduction in resistivity; a positive change is an increase in resistivity. *Level 1* and *level 7* are the uppermost level and bottommost levels, respectively. Each *spoke* represents data for a monitoring well

changes were detected at nearly all localities within the wells demonstrate that the field site is highly fractured with a degree of weathering insufficient to impede a majority of the fluid flow. Therefore, the field test using cross-hole ERT provides information about lateral and vertical flow that cannot be predicted on the basis of the well logs.

Summary and conclusions

Surface ERT imaged three-dimensional resistivity changes caused by dilution of the preexisting KCl plume on a broad scale during a tracer test in fractured basalt in Moscow, Idaho, USA. Surface ERT provided very useful information on the changes in resistivity due to the general pattern of water movement during tap-water injection and seasonal recharge, and on the stratigraphy that influenced water movement. However, individual fractures and fracture zones could not be distinguished; surface ERT is not capable of tracing the details of water movement at as small a scale as the cross-borehole technique also used here due to the decreased sensitivity with depth resulting from method application.

Cross-borehole ERT between an injection well containing the source solution, and seven nearby monitoring wells provided detailed information near the wells on the evolutionary plume dynamics during a diluting tracer test in fractured basalt. Cross-borehole ERT resistivities near the injection well delineated specific locations over time,

 DOI 10.1007/s10040-007-0159-z

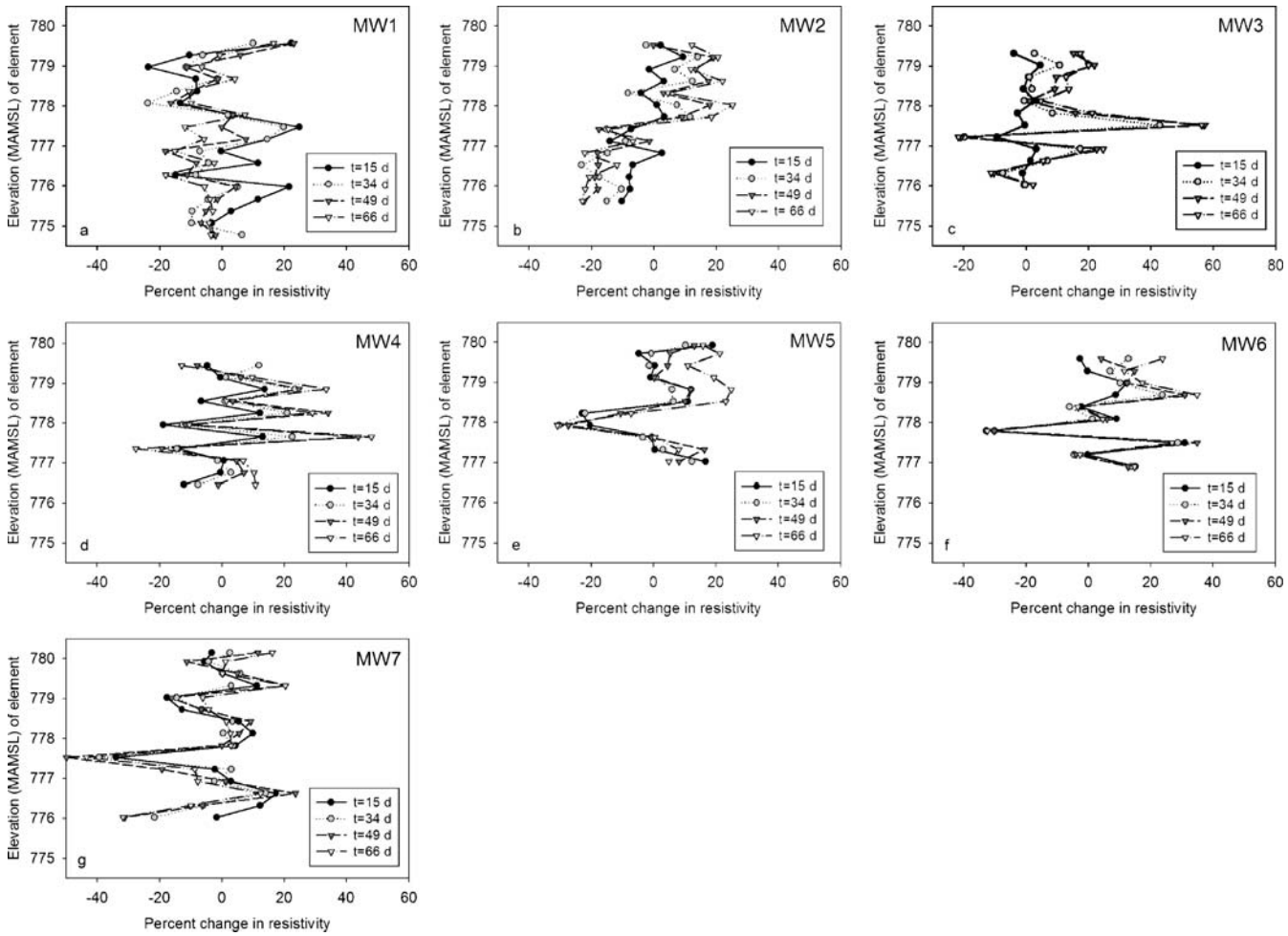

Fig. 9 Graphs of monitoring well inverted resistivities as percent change in resistivity from baseline for elements adjacent to the borehole within the subgrid region for the cross-borehole experiments (see example locations in Fig. 3). Phase 2 data are represented by *circles*; phase 3 data are represented by *upside-down triangles*. Note the shift in scale for the *MW3 x-axis* compared to the graphs for the other wells

where tap water exited the borehole reflecting fluid transmitting fractures or fracture zones. Cross-borehole ERT resistivities near the monitoring wells demarcate specific locations of resistivity change over time due to movement of different conductivity waters through fractures. Differentiation of high resistivities or resistivity tendencies over time caused by the influx of tap water or recharge water through analysis of the cross-borehole ERT data could not be achieved in most instances. Given the complexities of the experiment, cross-borehole ERT provided a great deal of lithologic information that would have been homogenized in a strictly hydrologic method analysis. ERT data clearly show the heterogeneous migration patterns of the solutions and mechanisms of solute transport in fractured basalt.

The results of this study indicate the application of surface and cross-borehole ERT may be adequate techniques for monitoring organic contaminants or natural recharge, depending on the conductivity contrast, for municipal water supplies, contaminant assessments, and source-water protection. Surface ERT may initially be used to cover large areas on an exploratory basis followed by cross-borehole ERT to more accurately focus on the specific area of interest.

Characterization of a shallow hydrogeologic system in fractured basalt was achieved from electrical resistivity data and hydraulic data collected during the tracer test. The slow flow rate of the artificial injection implies small-aperture fractures and/or fractures of unknown size filled with clay. The cross-borehole ERT data indicate that the field site is highly fractured; fractures are void of significant weathering and support both fast and slow flow paths. A hydraulic connection exists between the basalt and surface recharge, expected in areas where the clay layer or clay infilling is absent. The cross-borehole ERT data yield important information about anisotropic flow that could not be gleaned from well-log data, SP data, surface ERT, or MALM data, as those methods also were applied in this study.

Acknowledgements This investigation was conducted with generous financial support from Lockheed Martin Idaho Technologies, Inc., grant number C95175698-017 and Bechtel BWXT Idaho, LLC, grant number C95175698-017-001. Their support and counsel are greatly appreciated.

 DOI 10.1007/s10040-007-0159-z

References

Binley A, Ramirez A, Daily W (1995) Regularized image reconstruction of noisy electrical resistance tomography data. In: Bech MS et al. (eds) Process tomography. Proceedings of the 4th Workshop of the European Concerted Action on Process Tomography, Bergen, Norway, 6–8 April 1995, pp 401–410

Bush J, Seward WP (1992) Geologic field guide to the Columbia River Basalt, northern Idaho and southeastern Washington. Idaho Geol Surv Inform Circ 49

Chambers J, Ogilvy R, Meldrum P, Nissen J (1999) 3D resistivity imaging of buried oil- and tar-contaminated waste deposits. Eur J Environ Eng Geophys 4:3–15

Dahlin T, Bernstone C, Loke MH (2002) Case history: a 3-D resistivity investigation of a contaminated site in Lernacken, Sweden. Geophysics 67(6):1692–1700

Daily W, Ramirez A (1995) Electrical resistance tomography during in-situ trichloroethylene remediation at the Savannah River Site. J Appl Geophys 33:239–249

Daily W, Ramirez AL (2000) Electrical imaging of engineered hydraulic barriers. Geophysics 65(1):83–94

Daily W, Ramirez A, LaBrecque D, Nitao J (1992) Electrical resistivity tomography of vadose water movement. Water Resour Res 28(5):1429–1442

Daily W, Ramirez AL, LaBrecque D, Binley AM (1995a) Detecting leaks in hydrocarbon storage tanks using electrical resistance tomography, UCRL-JC-120547; CONF-9511130-1, p. 14, Presented at Frontiers'95, San Luis Obispo, CA, Nov. 1995

Daily W, Ramirez A, LaBrecque D, Barber W (1995b) Electrical resistance tomography experiments at the Oregon Graduate Institute. J Appl Geophys 33:227–237

deGroot Hedlin C, Constable S (1990) Occam's inversion to generate smooth, two-dimensional models from magnetotelluric data. Geophysics 55(12):1613–1624

Kemna A, Vanderborght J, Kulessa B, Vereecken H (2002) Imaging and characterisation of subsurface solute transport using electrical resistivity tomography (ERT) and equivalent transport models. J Hydrol 267:125–146

LaBrecque DJ, Ramirez AL, Daily WD, Binley AM, Schima SA (1996) ERT monitoring of environmental remediation processes. Measure Sci Technol 7(3):375–383

Li T (1990) Hydrogeologic characterization of a multiple aquifer fractured basalt system. PhD Thesis, University of Idaho, Moscow, ID, USA

Li Y, Oldenburg DW (1992) Approximate inverse mapping in DC resistivity problems. Geophys J Int 109:343–362

Loke MH (2001) RES3DINV, 3D Resistivity and IP Inversion software, Geotomo Software, Penang, Malaysia

Loke MH, Barker RD (1996) Lease squares inversion of apparent resistivity pseudosections by a quasi-Newton method. Geophys Prospect 44(1):131–152

Lundegard PD, LaBrecque D (1995) Air sparging in a sandy aquifer (Florence, Oregon, USA): actual and apparent radius of influence. J Contam Hydrol 19(1):1–27

Nimmer RE, Osiensky JL (2002a) Using mise-à-la-masse to delineate the migration of a conductive tracer in partially saturated basalt. Environ Geosci 9(2):81–87

Nimmer RE, Osiensky JL (2002b) Direct current and self potential monitoring of an evolving plume in partially saturated fractured rock. J Hydrol 267(3–4):258–272

Ogilvy R, Meldrum P, Chambers J (1999) Imaging of industrial waste deposits and buried quarry geometry by 3-D resistivity tomography. Eur J Environ Eng Geophys 3:103–113

Park S (1998) Fluid migration in the vadose zone from 3-D inversion of resistivity monitoring data. Geophysics 63(1):41–51

Park SK, Van GP (1991) Inversion of pole-pole data for 3-D resistivity structure beneath arrays of electrodes. Geophysics 56 (7):951–960

Provant AP (1995) Geology and Hydrogeology of the Viola and Moscow west quadrangles; Latah County, Idaho and Whitman County, Washington, MSc Thesis, University of Idaho, Moscow, ID, USA

Ramirez A, Daily W, LaBrecque D, Owen E, Chesnut D (1993) Monitoring an underground steam injection process using electrical resistance tomography. Water Resour Res 29(1):73–87

Ramirez A, Daily W, Binley A, LaBrecque D, Roelant D (1996) Detection of leaks in underground storage tanks using electrical resistance methods. J Environ Eng Geophys 1(3):189–203

Sasaki Y (1992) Resolution of resistivity tomography inferred from numerical simulation. Geophys Prospect 40:453–463

Singa K, Gorelick SM (2005) Saline tracer visualized with three-dimensional electrical resistivity tomography: Field-scale spatial moment analysis. Water Resour Res 41:W05023

Slater L, Binley A (2003) Evaluation of permeable reactive barrier (PRB) integrity using electrical imaging methods. Geophysics 68(3):911–921

Slater LD, Binley A, Brown D (1997a) Electrical imaging of fractures using groundwater salinity change. Ground Water 35 (3):436–442

Slater L, Zaidman MD, Binley AM, West LJ (1997b) Electrical imaging of saline tracer migration for the investigation of unsaturated zone transport mechanisms. Hydrol Earth Syst Sci 1 (2):291–302

Zaidman MD, Middleton RT, West LJ, Binley AM (1999) Geophysical investigation of unsaturated zone transport in the Chalk in Yorkshire. Q J Eng Geol 32:185–198

 DOI 10.1007/s10040-007-0159-z